Int. J. Solids Structures Vol. 21, No. 12, pp. 1213–1229, 1985
Printed in Great Britain.

0020-7683/85 $3.00 + .00
© 1985 Pergamon Press Ltd.

ON THE LOAD TRANSFER FROM A RIGID CYLINDRICAL INCLUSION INTO AN ELASTIC HALF SPACE

A. P. S. SELVADURAI† and R. K. N. D. RAJAPAKSE‡
Department of Civil Engineering, Carleton University, Ottawa, Ontario, Canada K1S 5B6

(*Received* 19 *July* 1984; *in revised form* 30 *January* 1985)

Abstract—The present paper examines the problems related to the axial, lateral, and rotational loading of a rigid cylindrical inclusion which is embedded in bonded contact at the boundary of an isotropic elastic half space. The rigid inclusion is modeled as a field of distributed forces which represent the normal and shear tractions that act on the inclusion–elastic-medium interface. The intensities of these distributed tractions are determined by enforcing displacement compatibility conditions at discrete locations of the interface. These compatibility conditions are derived from rigid-body displacement modes appropriate for each loading. The results derived from this numerical scheme are compared with equivalent results derived via analytical techniques which focus on the solution of the governing integral-equation schemes and other approximate-solution schemes. The numerical results presented in the paper illustrate the manner in which the generalized stiffnesses of the embedded inclusion are influenced by its geometry and Poisson's ratio of the half-space region.

INTRODUCTION

The category of problems that examine the behaviour of cylindrical inclusions which are either fully or partially embedded in elastic media have several useful engineering applications. Particularly in the field of geomechanics, the partially embedded cylindrical inclusion, models the behaviour of cylindrical piles or piers embedded in soil media which exhibit a linear elastic response in the working-load range. These inclusion problems are also of importance to the stress analysis of multiphase composites which are reinforced by elongated inclusions or fibres of finite length. The general interaction problem involves the action of four types of loading which induce axial and lateral translation, azimuthal rotation and asymmetric rotation about the axes of symmetry. To the authors knowledge, a rigorous analytical solution to the generalized three-dimensional problem involving a loaded finite rigid cylindrical inclusion is not available in the literature.

The seminal analytical work related to the load transfer from a cylindrical elastic inclusion of infinite length into an elastic medium is due to Muki and Sternberg[1]. These authors also presented an approximate procedure which can be used to determine the decay of load in a bar with an arbitrary cross-section. Based on the assumption that the bar behaves as a one-dimensional continuum, Muki and Sternberg[2] presented a solution scheme for axial load transfer from a finite elastic bar into an elastic half space. Luk and Keer[3] presented an exact analytical formulation for the problem of a rigid cylindrical inclusion partially embedded in an isotropic elastic half space. A Hankel transform development of the governing equations yields a system of coupled singular integral equations for the normal and shear traction distributions at the inclusion–elastic-medium interface. In an earlier paper Freeman and Keer[4] examined the problem of the transfer of torque from a semi-infinite elastic inclusion into an elastic half space. Spillers and Stoll[5] considered the problem of lateral loading of an elastic pile which is embedded in an elastic half space by treating the pile as a line inclusion obeying the Bernoulli–Euler beam theory. The interactive reaction between the pile and half space is modeled by the horizontal analog of the Mindlin force problem[6].

† Professor and Chairman.
‡ Post Doctoral Fellow.

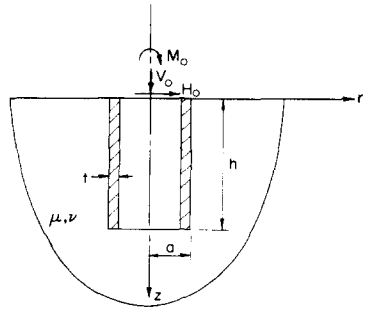

Fig. 1. Hollow rigid pier embedded in an elastic half space.

Poulos and Davis[7, 8], extended the work of Spillers and Stoll[5] to include axial loading of incompressible piles. Mindlin's solution[9] for a concentrated axial load was used to model the vertical stress acting on the interface. Suriyamongkol *et al.*[10] also investigated the behaviour of an axially loaded rigid cylindrical body embedded in an elastic half space. Recently Niumpradit and Karasudhi[11] and Apirathvorakij and Karasudhi[12] extended the scheme of Muki and Sternberg[2] to include the quasistatic axial load transfer and bending problems for an elastic bar partially embedded in a saturated poroelastic half space. Fowler and Sinclair[13] have also applied the analytical scheme proposed by Muki and Sternberg[2] to study the elastodynamic problem involving longitudinal vibrations. Parnes[14] considered the case of an infinite elastic bar embedded in an infinite space and subjected to an infinite train of periodic axial forces. Herrmann *et al.*[15] investigated the transfer of load from a microfibre into an elastic medium. Recently Selvadurai[16] and Au and Selvadurai[17] examined the problem of the lateral loading of a Bernoulli–Euler beam embedded in an isotropic infinite space. The solutions corresponding to rigid cylindrical and spheroidal inclusions embedded in elastic infinite space are presented in [18] and [19]. The above review is by no means extensive; references to further work are given by Sternberg[20] and Gladwell[21].

This paper focusses on the estimation of axial, lateral, rotational and coupled stiffnesses of a hollow rigid cylindrical inclusion embedded in a homogeneous isotropic elastic half space and subjected to a system of loading, as shown in Figure 1. The problem could be formulated in a manner similar to that of Luk and Keer[3], but leads to considerable analytical difficulties and needs tedious procedures in numerical implementation. In the present study we employ a scheme identical to that considered in [10] for axial loading. By presenting extensive comparisons we establish the fact that the present method is as accurate as the rigorous treatment of Luk and Keer for axial loading. At the same time, we present numerical values obtained from other schemes to complete the comparisons. Finally, the stiffnesses of a rigid inclusion are presented for different aspect ratios of the inclusion and Poisson ratio of the surrounding half space.

2. FUNDAMENTAL SOLUTIONS

Fig. 2 shows a half-space region in which (r, θ, z) is the cylindrical polar coordinate system and the related rectangular Cartesian coordinate system (x, y, z) is such that the z-axis is normal to the free surface. For an isotropic linear elastic medium, the displacement equations of equilibrium take the form

$$\nabla^2 u + \frac{1}{1-2\nu}\frac{\partial \Delta}{\partial r} - \frac{1}{r}\left(2\frac{\partial v}{r\partial\theta} + \frac{u}{r}\right) = 0, \tag{1a}$$

$$\nabla^2 v + \frac{1}{1-2\nu}\frac{\partial \Delta}{r\partial\theta} - \frac{1}{r}\left(\frac{v}{r} - 2\frac{\partial u}{r\partial\theta}\right) = 0, \tag{1b}$$

$$\nabla^2 w + \frac{1}{1-2\nu}\frac{\partial \Delta}{\partial z} = 0. \tag{1c}$$

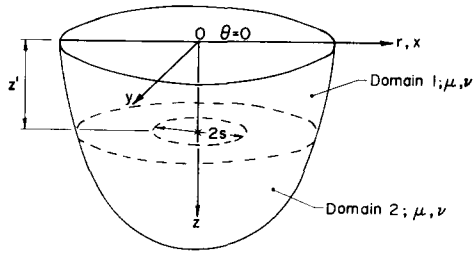

Fig. 2. System considered in deriving fundamental solution.

Where u, v and w are the components of the displacement vector referred to the cylindrical polar coordinate system, ν is the Poisson's ratio, ∇^2 and Δ are the Laplacian operator and dilatation, respectively, defined by

$$\nabla^2 = \frac{\partial^2}{\partial r^2} + \frac{1}{r}\frac{\partial}{\partial r} + \frac{1}{r}\frac{\partial^2}{\partial \theta^2} + \frac{\partial^2}{\partial z^2}, \tag{2a}$$

$$\Delta = \frac{\partial u}{\partial r} + \frac{u}{r} + \frac{\partial v}{r\partial\theta} + \frac{\partial w}{\partial z}. \tag{2b}$$

Muki[22] has presented a Fourier (in terms of θ)–Hankel (in terms of r) representation of the general solution of eqns (1) by expressing the displacements in terms of a combination of a biharmonic and harmonic functions. Accordingly, the displacements u, v, and w can be expressed as

$$u = \frac{1}{2}\sum_{m=0}^{\infty} [U_{m+1}(r, z) - V_{m-1}(r, z)] \cos m\theta, \tag{3a}$$

$$v = \frac{1}{2}\sum_{m=0}^{\infty} [U_{m+1}(r, z) + V_{m-1}(r, z)] \sin m\theta, \tag{3b}$$

$$w = \sum_{m=0}^{\infty}\left[\int_0^{\infty}\left\{(1-2\nu)\frac{d^2G_m}{dz^2} - 2(1-\nu)\xi^2 G_m\right\}\xi J_m(\xi r)\, d\xi\right]\cos m\theta, \tag{3c}$$

where, for each harmonic m,

$$U_{m+1}(r, z) = \int_0^{\infty}\left(\frac{dG_m}{dz} + 2H_m\right)\xi^2 J_{m+1}(\xi r)\, d\xi, \tag{4a}$$

$$V_{m-1}(r, z) = \int_0^{\infty}\left(\frac{dG_m}{dz} - 2H_m\right)\xi^2 J_{m-1}(\xi r)\, d\xi, \tag{4b}$$

$$G_m(\xi, z) = (A_m + B_m z)\, e^{\xi z} + (C_m + D_m z)\, e^{-\xi z}, \tag{4c}$$

$$H_m(\xi, z) = E_m\, e^{\xi z} + F_m\, e^{-\xi z}. \tag{4d}$$

In eqns (4), J_m is the Bessel function of the first kind of the mth order and $A_m(\xi)$, $B_m(\xi)$, . . . , $F_m(\xi)$ are arbitrary functions which should be determined by invoking appropriate boundary and/or continuity conditions. At this stage, it is convenient to nondimensionalise the problem by defining a length parameter "a" which denotes the external radius of the rigid cylindrical inclusion; a is taken as a unit length.

In order to develop the solutions corresponding to appropriate ring loads of finite extent, acting on the contact surface of the inclusion, it is necessary to derive expressions for the displacements due to concentrated circular ring loads of unit intensity as shown in Fig. 3. These loads are assumed to act along the circumference of a circle with radius equal to s at the interior of half space at $z = z'$. By defining a fictitious plane at $z = z'$, we can reduce the problem to one which has two domains (Fig. 2).

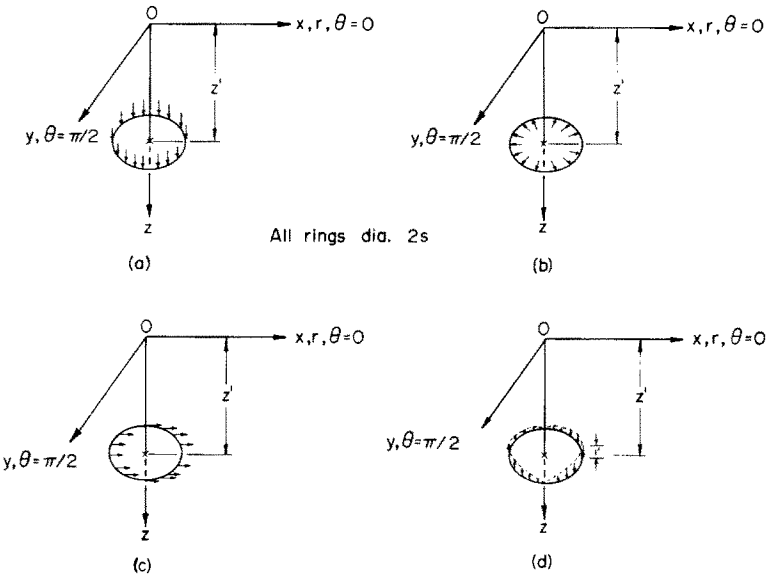

Fig. 3. Concentrated ring forces of unit intensity.

The superscript $i(i = 1, 2)$ is used to identify the quantities associated with each domain. The displacement field in each domain has the general form given by eqns (3) consisting of functions $A_i(\xi)$, $B_i(\xi)$, . . . , $F_i(\xi)$. In the domain 2 however, to ensure regularity of displacements and stresses derived from eqns (2), the terms $A_2(\xi)$, $B_2(\xi)$, $E_2(\xi)$ are set equal to zero. The remaining functions are determined from the boundary, continuity and symmetry conditions appropriate to each loading case.

Concentrated vertical ring force [Fig. 3(a)]

The system under consideration possesses a state of symmetry about the z-axis and the corresponding displacements are given by eqns (3) with $m = 0$. Thus the displacement v in θ direction vanishes and the arbitrary constants $A_1(\xi)$, $B_1(\xi)$, $C_1(\xi)$, $D_1(\xi)$, $C_2(\xi)$ and $D_2(\xi)$ are determined from the following boundary and continuity conditions:

$$\sigma_{zz}^{(1)}(r, 0) = 0, \tag{5a}$$

$$\sigma_{zr}^{(1)}(r, 0) = 0, \tag{5b}$$

$$u^{(1)}(r, z') = u^{(2)}(r, z'), \tag{5c}$$

$$w^{(1)}(r, z') = w^{(2)}(r, z'), \tag{5d}$$

$$\sigma_{zz}^{(1)}(r, z') - \sigma_{zz}^{(2)}(r, z') = \delta(r - s) = \int_0^\infty s\xi J_0(\xi s)J_0(\xi r)\, d\xi, \tag{5e}$$

$$\sigma_{zr}^{(1)}(r, z') - \sigma_{zr}^{(2)}(r, z') = 0. \tag{5f}$$

Concentrated radial ring force [Fig. 3(b)]

As noted previously, the system possesses symmetry about the z-axis and the appropriate boundary and continuity conditions are identical to those given in eqns (5) except that eqns (5e) and (5f) should be changed to the following:

$$\sigma_{zz}^{(1)}(r, z') - \sigma_{zz}^{(2)}(r, z') = 0, \tag{6a}$$

$$\sigma_{zr}^{(1)}(r, z') - \sigma_{zr}^{(2)}(r, z') = \delta(r - s) = \int_0^\infty s\xi J_1(\xi s)J_1(\xi r)\, d\xi. \tag{6b}$$

Concentrated ring force in x direction [Fig. 3(c)]

The system under consideration possesses symmetry about the $\theta = 0$ axis, and the displacements are obtained from eqns (3) with a single term in the series with $m = 1$. Thus there are nine functions $A_1(\xi)$, $B_1(\xi)$, $C_1(\xi)$, $D_1(\xi)$, $E_1(\xi)$, $F_1(\xi)$, $C_2(\xi)$, $D_2(\xi)$ and $F_2(\xi)$ to be determined from the following boundary and continuity conditions:

$$\sigma_{zz}^{(1)}(r, \theta, 0) = 0, \tag{7a}$$

$$\sigma_{zr}^{(1)}(r, \theta, 0) = 0, \tag{7b}$$

$$\sigma_{z\theta}^{(1)}(r, \theta, 0) = 0, \tag{7c}$$

$$u^{(1)}(r, \theta, z') = u^{(2)}(r, \theta, z'), \tag{7d}$$

$$v^{(1)}(r, \theta, z') = v^{(2)}(r, \theta, z'), \tag{7e}$$

$$w^{(1)}(r, \theta, z') = w^{(2)}(r, \theta, z'), \tag{7f}$$

$$\sigma_{zz}^{(1)}(r, \theta, z') = \sigma_{zz}^{(2)}(r, \theta, z'), \tag{7g}$$

$$[\sigma_{z\theta}^{(1)}(r, \theta, z') - \sigma_{z\theta}^{(2)}(r, \theta, z')]/\sin\theta + [\sigma_{zr}^{(1)}(r, \theta, z') - \sigma_{zr}^{(2)}(r, \theta, z')]/\cos\theta = 0, \tag{7h}$$

$$[\sigma_{z\theta}^{(1)}(r, \theta, z') - \sigma_{z\theta}^{(2)}(r, \theta, z')]/\sin\theta - [\sigma_{zr}^{(1)}(r, \theta, z') - \sigma_{zr}^{(2)}(r, \theta, z')]/\cos\theta = -2\delta(r - s) = -\int_0^\infty s\xi J_0(\xi s) J_0(\xi r)\, d\xi. \tag{7i}$$

Concentrated vertical ring force with asymmetric distribution [Fig. 3(d)]

Again, the system possesses symmetry about $\theta = 0$ axis and the displacements are obtained from eqns (3) where $m \equiv 1$. The appropriate boundary and continuity conditions are identical to those given in eqns (7), except that eqns (7g) and (7i) should be changed to the following:

$$[\sigma_{zz}^{(1)}(r, \theta, z') - \sigma_{zz}^{(2)}(r, \theta, z')] \cos\theta = \delta(r - s) = \int_0^\infty s\xi J_1(\xi s) J_1(\xi r)\, d\xi, \tag{8a}$$

$$[\sigma_{z\theta}^{(1)}(r, \theta, z') - \sigma_{z\theta}^{(2)}(r, \theta, z')]/\sin\theta - [\sigma_{zr}^{(1)}(r, \theta, z') - \sigma_{zr}^{(2)}(r, \theta, z')]/\cos\theta = 0. \tag{8b}$$

The boundary and continuity conditions given in eqns (5)–(8) result in sets of simultaneous equation systems corresponding to the four different cases of loading shown in Fig. 3. The solution of these systems leads to the expressions for arbitrary functions appropriate to each loading case. The expressions for displacements corresponding to each loading case are presented in the Appendix [eqns (A1)–(A10)].

3. A HOLLOW RIGID INCLUSION EMBEDDED IN THE HALF SPACE

We consider the problem of a hollow rigid cylinder or inclusion embedded in a homogeneous elastic half space and subjected to the system of external loads as shown in Fig. 4. It is assumed that the boundary of the hollow rigid cylinder is perfectly bonded to the surrounding elastic medium. In order to evaluate the stress distributions and stiffnesses of the inclusion we discretize the axisymmetric interface surface by regions of uniform or linearly varying tractions (Fig. 4). It may be observed that the cylinder–elastic-medium interface of any rigid pier can be discretized by using combination of the two ring elements shown in Fig. 5. These are identified as shaft elements (SE) and base elements (BE). In the case of a SE it is assumed that the tractions are distributed uniformly across the thickness of an element. However, the symmetric radial tractions acting on a BE under axial loading, and asymmetric normal traction acting on a BE under lateral and moment loading, are assumed to have a linear variation across the width of an element. This would enhance the integration of corresponding funda-

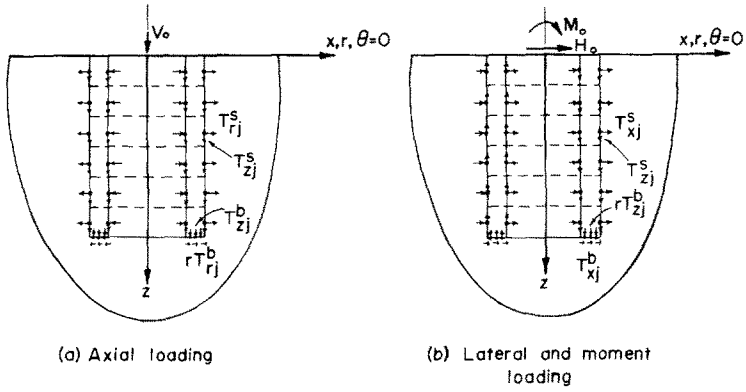

Fig. 4. Distributed forces acting on the contact surface of cylinder.

mental solutions across the element thickness. The unknown tractions acting on jth element is denoted by $T^n_{mj}(m = r, x, z, n = s, b)$ where subscript m denotes the direction of traction and superscript n is used to identify whether the element is a shaft element or a base element. The influence function $[f(r_i, z_i, s_j, z_j)]^{mn}_q(q = r, x, z, m = r, x, z, n = s, b)$ denotes the displacement in the m direction at a point $P_i(r_i, z_i)$ due to a unit traction acting in q direction on the jth element. The superscript n is used to identify whether the jth element is a shaft element or a base element. The expressions for $[f(r_i, z_i, s_j, z_j)]^{mn}_q$ are presented in eqns (A11)–(A18) and (A24)–(A31) in the Appendix. In what follows we establish the flexibility equations of the inclusion under axial, lateral and moment loading.

Axial loading

Under the action of an axial load the contact surface of the cylinder is subjected to unknown stresses acting in the vertical and radial directions [Fig. 4(a)]. Because we assume that this stress field is generated by the integration of fundamental concentrated ring loads shown in Figs. 3(a) and 3(b), the stress-free boundary conditions at $z = 0$ is automatically satisfied. The boundary conditions which remain to be satisfied are those associated with the displacements of the contact surface of the inclusion which can be expressed as

$$w(a, z) = \Delta_v; \qquad u(a, z) = 0 \qquad (0 \le z \le h), \tag{9a}$$

$$w(a - t, z) = \Delta_v; \qquad u(a - t, z) = 0 \qquad (0 \le z \le h), \tag{9b}$$

$$w(r, h) = \Delta_v; \qquad u(r, h) = 0 \qquad (t - a \le r \le a), \tag{9c}$$

where Δ_v is the vertical displacement of the inclusion under the load V_0.

The displacements $u_i(r_i, z_i)$ and $w_i(r_i, z_i)$ at point $P_i(r_i, z_i)$ due to the stress field

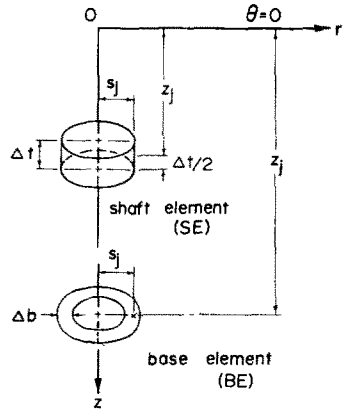

Fig. 5. Geometry of a shaft element and a base element.

acting on the contact surface can be expressed as

$$u_i(r_i, z_i) = \sum_{j=1}^{N_s} \{[f(r_i, z_i, s_j, z_j)]_z^{rs} T_{zj}^s + [f(r_i, z_i, s_j, z_j)]_r^{rs} T_{rj}^s\} + \sum_{j=1}^{N_b} \{[f(r_i, z_i, s_j, z_j)]_z^{rb} T_{zj}^b + [f(r_i, z_i, s_j, z_j)]_r^{rb} T_{rj}^b\}, \quad (10a)$$

$$w_i(r_i, z_i) = \sum_{j=1}^{N_s} \{[f(r_i, z_i, s_j, z_j)]_z^{zs} T_{zj}^s + [f(r_i, z_i, s_j, z_j)]_r^{zs} T_{rj}^s\} + \sum_{j=1}^{N_b} \{[f(r_i, z_i, s_j, z_j)]_z^{zb} T_{zj}^b + [f(r_i, z_i, s_j, z_j)]_r^{zb} T_{rj}^b\}, \quad (10b)$$

where N_s and N_b are the number of shaft and base elements, respectively. If we impose the boundary conditions given by eqns (9) with $\Delta_v = 1$ in eqns (10), a system of simultaneous equations of order $2(N_s + N_b)$ is formed with $T_{zj}^s \ldots T_{rj}^b$ corresponding to each element as the unknown vector. The solution of this system of simultaneous equations gives the intensity of the distributed stress field acting on the rigid inclusion–elastic-medium interface. The applied vertical force can be expressed as

$$V_0 = \sum_{j=1}^{N_s} 2\pi r_j \Delta t \cdot T_{zj}^s + \sum_{j=1}^{N_b} 2\pi r_j \Delta b \cdot T_{zj}^b. \quad (11)$$

Lateral and moment loading

Under the action of a lateral or a moment loading, the stress and displacement fields are symmetrical about $\theta = 0$ or x axis. The contact surface of the cylindrical inclusion is subjected to unknown stresses acting in vertical (z) and horizontal (x) directions [Fig. 4(b)]. As in the previous case, we assume that this stress field is generated by the integration of fundamental concentrated ring loads shown in Fig. 3(c) and 3(d). The stress-free boundary conditions at $z = 0$ are automatically satisfied. The boundary conditions which remain to be satisfied are those associated with the displacements at the contact surface of the inclusion along the plane $\theta = 0$ which can be expressed as

$$w(a, z) = a\phi_0 \quad (0 \le z \le h), \quad (12a)$$

$$w(a - t, z) = (a - t)\phi_0 \quad (0 \le z \le h), \quad (12b)$$

$$w(r, h) = r\phi_0 \quad (a - t \le r \le a), \quad (12c)$$

$$u(a, z) = \Delta_h - z\phi_0 \quad (0 \le z \le h), \quad (13a)$$

$$u(a - t, z) = \Delta_h - z\phi_0 \quad (0 \le z \le h), \quad (13b)$$

$$u(r, h) = \Delta_h - h\phi_0 \quad (t - a \le r \le a), \quad (13c)$$

where Δ_h and ϕ_0 are the displacement in x direction at $z = 0$ and rotation of the cylinder, respectively. The displacements $u_i(r_i, z_i)$ and $w_i(r_i, z_i)$ at a point $P_i(r_i, z_i)$ on the $\theta = 0$ plane due to the stress field acting on the contact surface can be expressed as

$$u_i(r_i, z_i) = \sum_{j=1}^{N_s} \{[f(r_i, z_i, s_j, z_j)]_z^{xs} T_{zj}^s + [f(r_i, z_i, s_j, z_j)]_x^{xs} T_{xj}^s\} + \sum_{j=1}^{N_b} \{[f(r_i, z_i, s_j, z_j)]_z^{xb} T_{zj}^b + [f(r_i, z_i, s_j, z_j)]_x^{xb} T_{xj}^b\}, \quad (14a)$$

$$w_i(r_i, z_i) = \sum_{j=1}^{N_s} \{[f(r_i, z_i, s_j, z_j)]_z^{zs} T_{zj}^s + [f(r_i, z_i, s_j, z_j)]_x^{zs} T_{xj}^s\} + \sum_{j=1}^{N_b} \{[f(r_i, z_i, s_j, z_j)]_z^{zb} T_{zj}^b + [f(r_i, z_i, s_j, z_j)]_x^{zb} T_{xj}^b\}. \quad (14b)$$

Unlike in the axial loading case, if we impose the boundary conditions given in eqns (12) and (13) directly in eqns (14), the resulting system of simultaneous equations has one additional unknown because Δ_h and ϕ_0 are coupled under lateral as well as moment loading. Therefore, we express the displacement boundary conditions of u as

$$u_i(a, z_i) - u_{i+1}(a, z_{i+1}) = \Delta t\phi_0 \qquad (0 \le z_i, z_{i+1} \le h), \tag{15a}$$

$$u_i(r_i, h) - u_{i+1}(r_{i+1}, h) = 0 \qquad (t - a \le r_i, r_{i+1} \le a). \tag{15b}$$

If ith element is on the shaft and $(i + 1)$ element is on the base, then

$$u_i(a, z_i) - u_{i+1}(r_{i+1}, h) = \frac{\Delta t}{2}\phi_0. \tag{15c}$$

The substitution of eqns (14) in eqns (12) and (15), together with $\phi_0 = 1$, result in a system of simultaneous equations with $2(N_s + N_b) - 1$ equations. The remaining equation is obtained by considering the global equilibrium of the inclusion as follows:

$$\sum_{j=1}^{N_s} \{\pi r_j^2 \cdot \Delta t T_{zj}^s - 2\pi r_j z_j \cdot \Delta t T_{xj}^s\} + \sum_{j=1}^{N_b} \left\{\frac{\pi}{4}[(r_j + \Delta b/2)^4 - (r_j - \Delta b/2)^4]T_{zj}^b - 2\pi r_j h \cdot \Delta b T_{xj}^b\right\} = M_0, \tag{16a}$$

$$\sum_{j=1}^{N_s} 2\pi r_j \cdot \Delta t T_{xj}^s + \sum_{j=1}^{N_b} 2\pi r_j \cdot \Delta b T_{xj}^b = H_0. \tag{16b}$$

If the inclusion is subjected to only a horizontal load, then we use eqn (16a) with $M_0 = 0$ to obtain the additional equation to generate a proper system of simultaneous equations. If the inclusion is subjected to only a moment loading, then we use eqn (16b) with $H_0 = 0$ to obtain the required additional equation. Once the solution to the system of simultaneous equations are obtained, we can compute the value of the applied load M_0 or H_0 by using eqns (16). The horizontal displacement Δ_h of the inclusion at $z = 0$ is computed from the following:

$$\Delta_h = \sum_{j=1}^{N_s} \{[f(r_1, z_1, s_j, z_j)]_z^{xs} T_{zj}^s + [f(r_1, z_1, s_j, z_j)]_x^{xs} T_{xj}^s\} + \sum_{j=1}^{N_b} \{[f(r_1, z_1, s_j, z_j)]_z^{xb} T_{zj}^b + [f(r_1, z_1, s_j, z_j)]_x^{xb} T_{xj}^b\} + 0.5\,\Delta t. \tag{17}$$

4. NUMERICAL-SOLUTION SCHEME

The numerical solution of the system of simultaneous equations involves the computation of influence functions presented in eqns (A11)–(A18) and (A24)–(A31) in the Appendix. These influence functions consist of integrals of the Lipschitz–Hankel type[23] of the following form:

$$I(p, q, ;\lambda) = \int_0^\infty J_p(\xi r) J_q(\xi s) \xi^\lambda \, e^{-\zeta\xi} \, d\xi. \tag{18}$$

Eason *et al.*[24] examined these integrals and expressed them in terms of functions tabulated by Heuman[25]. The functions tabulated by Heuman are symbolically represented by F_0, E_0 and Λ_0. These functions are directly related to complete elliptic integrals of the first, second and third kind[26]. In evaluating the Lipschitz–Hankel-type integrals $I(m, n;p)$ appearing in the influence functions, we use the expression presented by Eason *et al.*[24] for $I(0, 0;0)$, $I(1, 1;0)$, $I(0, 0;1)$, $I(1, 1;1)$, $I(1, 0;-1)$,

$I(1, 0;0)$, $I(1, 0;-1)$ and $I(1, 1;-1)$ together with the following recurrence relationships[24]:

$$rI(p+1, q;\lambda) + sI(p, q+1;\lambda) = C_{p,q} + (p+q+\lambda)I(p, q;\lambda-1) - cI(p, q;\lambda), \quad (19)$$

$$rI(p-1, q;\lambda) + sI(p, q-1;\lambda) = -C_{p,q} + (p+q-\lambda)I(p, q;\lambda-1) + cI(p, q;\lambda), \quad (20)$$

$$rI(p-1, q;\lambda) - sI(p, q+1;\lambda) = -C_{p,q} + (p-q-\lambda)I(p, q;\lambda-1) + cI(p, q;\lambda). \quad (21)$$

where

$$C_{p,q} = \begin{cases} \dfrac{r^p s^q}{2^{p+q}\Gamma(p+1)\Gamma(q+1)} & \text{if } p+q+\lambda = 0, \\ 0 & \text{if } p+q+\lambda > 0. \end{cases} \quad (22)$$

The numerical values of F_0 and E_0 are computed by using the series expansion presented by Abramowitz and Stegun[26]. Since there are no such general expansions available for Λ_0, we employ Gaussian quadrature (formulae) with thirty-two quadrature points[26] to accurately estimate Λ_0.

Based on the above solution scheme and the associated numerical procedures, the authors have developed a computer code to evaluate the stiffness of rigid piers. The inputs to the program are the shear modulus and Poisson's ratio of the half space (μ, ν), length–radius ratio of the bar (h/a) wall thickness (t), number of shaft and base elements (N_s and N_b). The output contains intensity of stresses at node points, displacement of the cylinder at $z = 0$, and load transfer curves of the cylinder. It is observed that the ill-conditioning of the system of simultaneous equation occurs for long cylinders due to the contribution from base elements. The iterative solution scheme presented in [10] could be used under such conditions. This situation does not arise in the case of a shell, since there are no base elements with an area very small compared to shaft elements.

5. DISCUSSION AND CONCLUSIONS

Figure 6 shows the comparison of vertical displacement on the free surface of the half space with the results presented by Luk and Keer[3]. It is evident that the results agree very closely even for a very short shell and a rod. Table 1 presents comparison of vertical stiffness obtained from other available approximate schemes. The method of analysis presented by Poulos and Davis[7] where radial stresses and compatibility of radial displacement were neglected, agrees very closely except for a very short bar ($h/a = 0.5$). In the limiting case as time approaches infinity, the solution of Niumpradit and Karasudhi[11] corresponds to the case considered by Muki and Sternberg[2]. The results are in very close agreement for long bars. Recently Karasudhi, Rajapakse and Hwang[27] presented a new compatibility condition for torsion transfer from an elastic bar into a layered elastic half space. Instead of using a cross-sectional average as proposed by Muki and Sternberg[1], they proposed a compatibility near the interface of the interacting systems. Karasudhi, Rajapakse and Liyanage[28] reconsidered the axial, lateral and moment load transfer using this new compatibility condition. The numerical results are presented in Table 1, and they agree very closely with those obtained from the present scheme. Figure 7(a) presents comparison of load transfer curves under axial loading for a bar embedded in a half space with $\nu = 0.3$. The load transfer curve obtained from the present study for a bar with $h/a = 5.0$ agrees closely

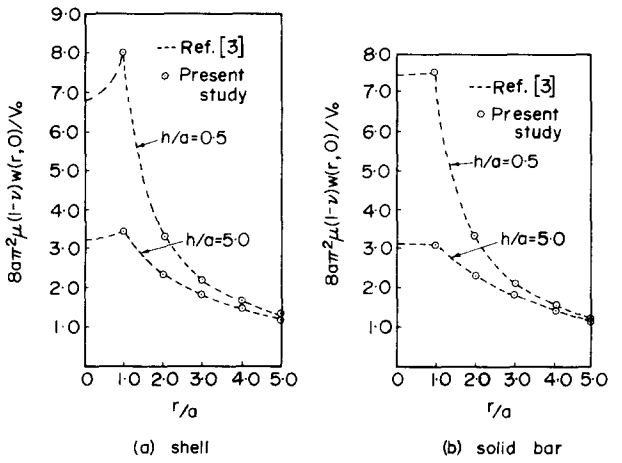

Fig. 6. Comparison of vertical displacement on surface of half space under axial loading: $\nu = 0.3$.

Table 1. Comparison of vertical stiffness of a solid bar under a vertical load: ($\nu = 0.25$, $t = a$).

Method of analysis	$V_0/\mu a\Delta_v$			
	$h/a = 0.5$	$h/a = 5.0$	$h/a = 10.0$	$h/a = 20.0$
Present study	7.06	17.02	24.80	38.96
Poulos type analysis	6.51	16.42	24.20	38.20
Niumpradit and Karasudhi[11]	—	—	24.73	39.96
Karasudhi et al.[28]	—	16.26	24.75	38.99

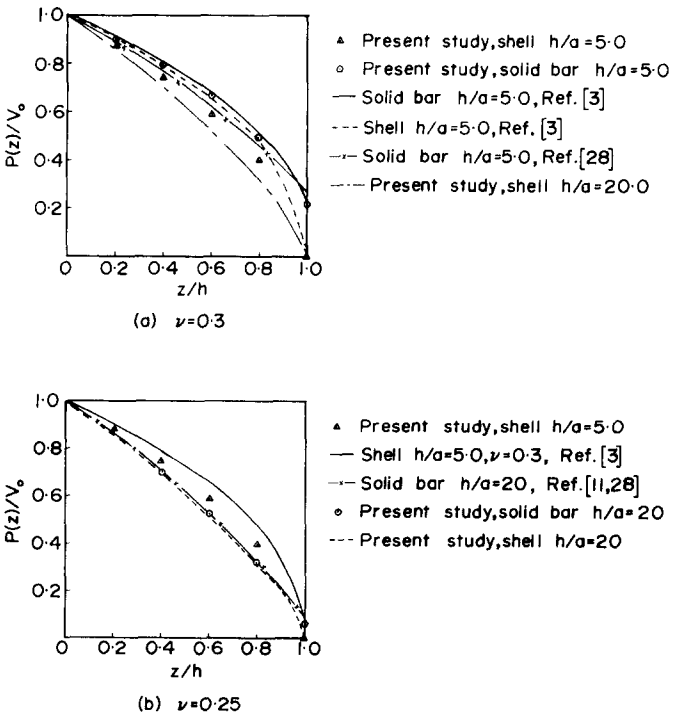

Fig. 7. Comparison of vertical load transfer curves.

Table 2. Comparison of translational stiffness of a solid bar under a lateral load: ($\nu = 0.25$, $t = a$).

Method of analysis	$H_0/\mu a\Delta_h$			
	$h/a = 0.5$	$h/a = 5.0$	$h/a = 10.0$	$h/a = 20.0$
Present study	6.10	10.01	12.80	18.40
Poulos type analysis	5.42	9.21	12.13	18.01
Apirathvorakij and Karasudhi[12]	—	8.30	10.67	16.33
Karasudhi et al.[28]	—	8.65	12.00	17.97

with that of Luk and Keer[3]. The load transfer curve corresponding to [28] shows a slight discrepancy and a higher percentage of load transfer at the base. However, it should be mentioned here that significant differences exist between the load transfer curve obtained from the present study and that given by Luk and Keer[3] for a shell of $h/a = 5.0$. In the present study we observe that the load transfer curves for shells observe a trend which is opposite to that observed by Luk and Keer[3]. The load transfer curve for a shell with $h/a = 20$, falls well below the load transfer curves for a shell and a rod with $h/a = 5.0$. This situation is clearly illustrated in Fig. 7(b), where we compare the load transfer curve for a shell and a rod with $h/a = 20$. Intuition suggests that as h/a increases, the load transfer curve of a shell should approach that of a solid bar. The load transfer curve for a solid bar with $h/a = 20$, obtained from present study, agrees very closely with those corresponding to [11, 28].

Tables 2, 3 and 4 present comparison of lateral, rotational and coupled stiffness of a solid bar with different geometric aspect ratios h/a. For long bars ($h/a \geq 10$), the results obtained from the four different methods agree closely. The solution scheme of Karasudhi *et al.*[28] agrees very closely with the results obtained from the present study for long bar ($h/a \geq 10$). The solution scheme of Apirathvorakij and Karasudhi[12] always results in a low value of translational, rotational and coupled stiffness. For bars with moderate to low h/a ratios ($h/a \leq 5.0$) where the solution schemes of [12, 28] are not applicable, Poulos'[29] analyses (see also [7, 8]) give considerable error for rotational and coupled stiffnesses. It would appear that in this range, accurate results could only be obtained from either an exact solution of the problem or via a discretization scheme as that presented here. The shear and moment distribution along the length for a bar with $h/a = 5.0$ is compared in Figs. 8 and 9 for moment loading and horizontal loading. The distribution of shear and moment follow similar trends except that slight differences

Table 3. Comparison of rotational stiffness of a solid bar under a moment: ($\nu = 0.25$, $t = a$).

Method of analysis	$M_0/100\mu a^3\phi_0$			
	$h/a = 0.5$	$h/a = 5.0$	$h/a = 10.0$	$h/a = 20.0$
Present study	0.08	1.54	6.67	34.70
Poulos type analysis	0.02	1.32	5.82	34.20
Apirathvorakij and Karasudhi[12]	—	1.23	5.31	31.25
Karasudhi et al.[28]	—	1.31	6.25	35.71

Table 4. Comparison of coupled stiffness of a solid bar under moment and lateral loading: ($\nu = 0.25$, $t = a$)

Method of analysis	$H_0/10Ea^2\phi_h$, $M_0/10Ea^2\Delta_m$			
	$h/a = 0.5$	$h/a = 5.0$	$h/a = 10.0$	$h/a = 20.0$
Present study	0.67	2.01	4.87	12.42
Poulos type analysis	0.17	1.69	4.31	11.97
Apirathvorakij and Karasudhi[12]	—	1.62	—	10.86
Karasudhi et al.[28]	—	1.75	4.36	12.04

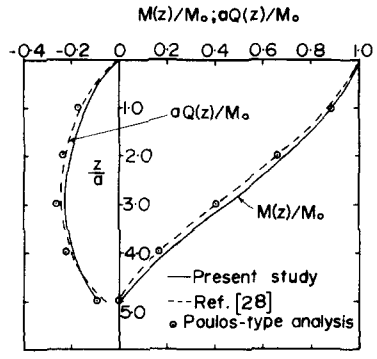

Fig. 8. Shear and moment distribution under moment loading: $h/a = 5.0$, $\nu = 0.25$.

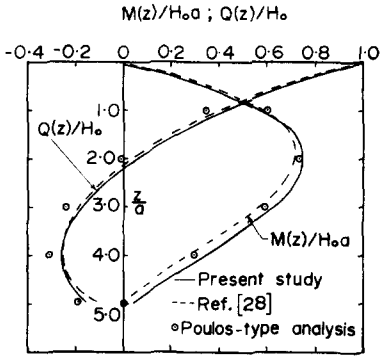

Fig. 9. Shear and moment distribution under horizontal loading: $h/a = 5.0$, $\nu = 0.25$.

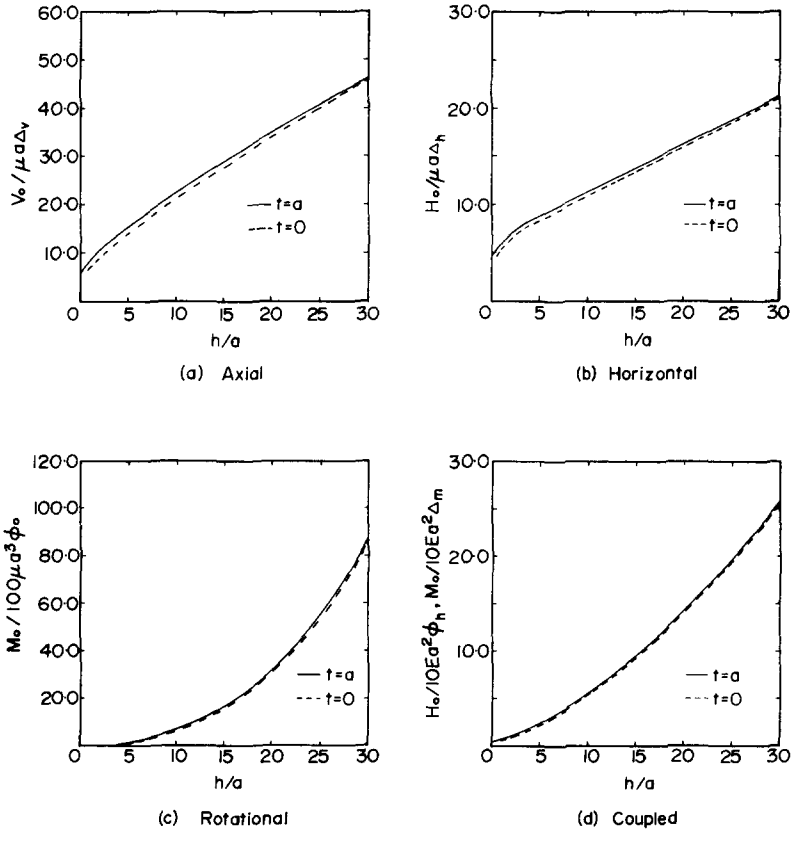

Fig. 10. Variation of stiffness with length–radius ratio: $\nu = 0.0$.

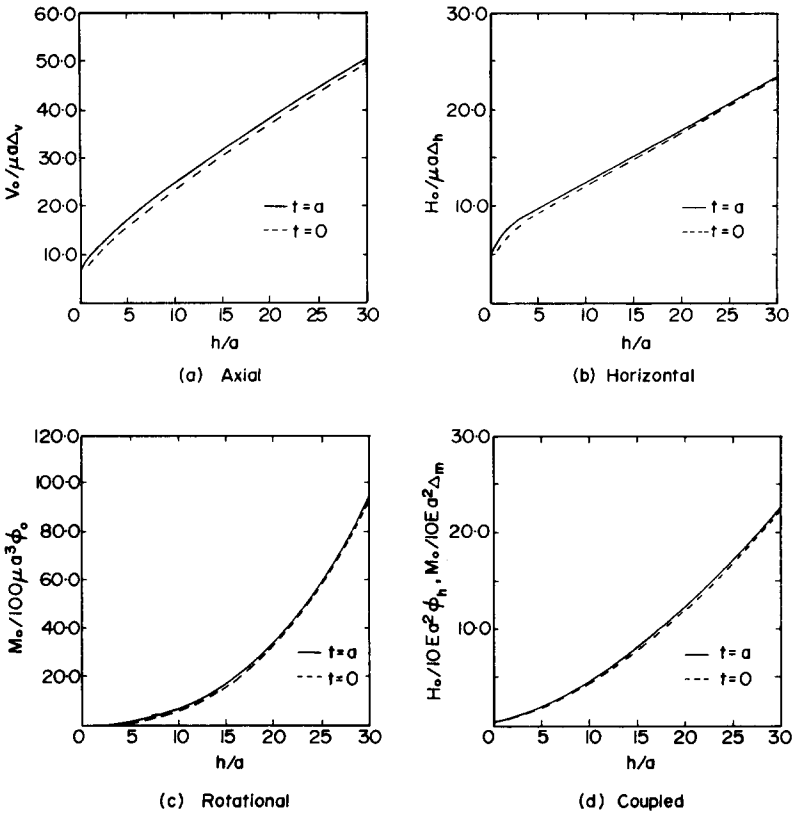

Fig. 11. Variation of stiffness with length–radius ratio: $\nu = 0.25$.

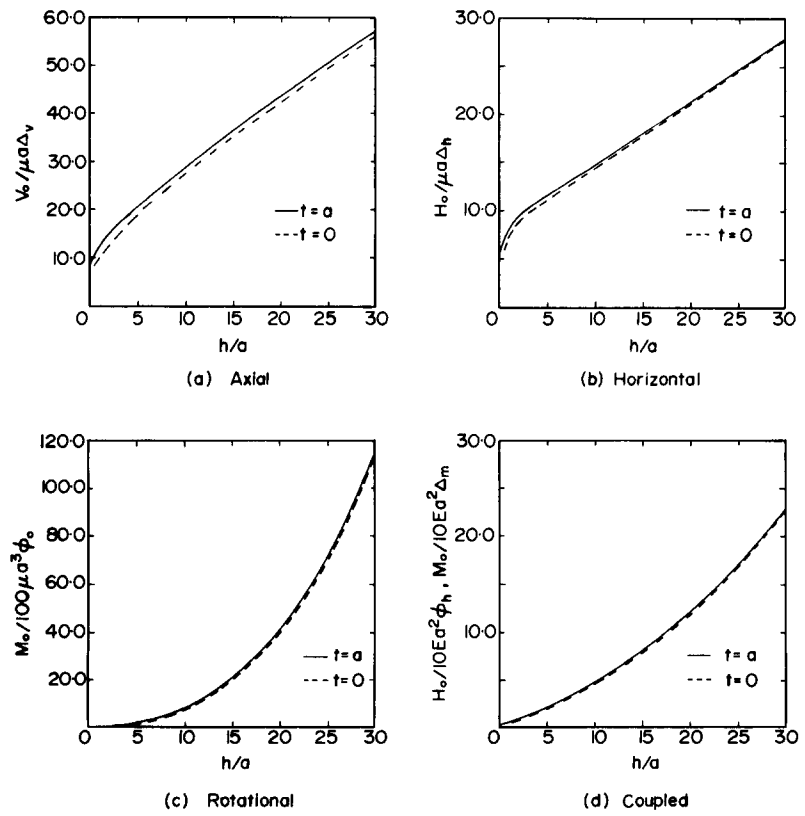

Fig. 12. Variation of stiffness with length–radius ratio: $\nu = 0.50$.

exist between the maximum values and also those at the base of the bar. It should be mentioned here that for bar with $h/a < 5$, considerable differences exist between distribution curves obtained from the present study and those by a scheme similar to Poulos[29].

One of the most important observations concerning the numerical results is that the stiffness of a shell is very close to that of a rigid bar. Even for $h/a = 0.5$, the difference is less than 10%. Figures 10–12 present the axial, translational, rotational and coupled stiffness of a solid cylinder and shell for different h/a ratios and Poisson's ratios of the surrounding half space. Since the stiffness of a shell is very close to that of a solid bar, we do not present results for a hollow cylinder. From these figures it is evident that an accurate estimate of the stiffness of a hollow cylinder could be obtained by considering solid cylinder of equal external diameter.

From the discussion of numerical results it can be concluded that the present method of analysis yields results which agree very closely with those presented by Luk and Keer[3] for vertical load transfer problems. However, we have observed considerable differences for load transfer curves for shells. The available approximate schemes presented in [2, 5, 7, 10–12, 28] could be considered as accurate methods for load transfer problems for a rigid bar with $h/a \geq 10$, under all types of loading. However, for moderate to short bars ($h/a \leq 5.0$), only the present method yields very accurate results when compared with Luk and Keer[3]. From the numerical point of view, the present method is computationally more efficient than the scheme employed by Luk and Keer[3] under general loading. However, for long bars, the solution scheme of Karasudhi *et al.*[28] can be considered computationally superior, besides the fact that such a scheme is applicable to both rigid and elastic bars.

Acknowledgements—The authors are grateful to Prof. Pisidhi Karasudhi of Asian Institute of Technology, Bangkok, for providing numerical results for comparison. The work described in this paper was supported by a Natural Sciences and Engineering Research Council of Canada Grant A3866 awarded to APSS.

REFERENCES

1. R. Muki and E. Sternberg, On the diffusion of an axial load from an infinite cylindrical bar embedded in an elastic medium. *Int. J. Solids Structures* **5**, 587 (1969).
2. R. Muki and E. Sternberg, Elastostatic load transfer to a half space from a partially embedded axially loaded rod. *Int. J. Solids Structures* **6**, 69 (1970).
3. V. K. Luk and L. M. Kerr, Stress analysis for an elastic half space containing an axially loaded rigid cylindrical rod. *Int. J. Solids Structures* **15**, 805 (1979).
4. L. M. Keer and N. J. Freeman, Load transfer problem for an embeded shaft in torsion. *J. Appl. Mech. ASME* **37**, 959 (1970).
5. W. R. Spillers and R. D. Stoll, Lateral response of piles. *J. Soil Mech. Found. ASCE* **90**, 1 (1964).
6. R. D. Mindlin and D. H. Cheng, Nuclei of strain in the semi-infinite solid. *J. Appl. Phys.* **21**, 926 (1950).
7. H. G. Poulos and E. H. Davis, The settlement behavior of single axially loaded incompressible piles and piers. *Geotechnique* **18**, 351 (1968).
8. H. G. Poulos and E. H. Davis, *Pile Foundation Analysis and Design*. Wiley, New York (1980).
9. R. D. Mindlin, Force at a point in the interior of a semi-infinite solid. *Physics* **7**, 195 (1936).
10. S. Suriyamongkol, P. Karasudhi and S. L. Lee, Axially loaded rigid cylindrical body embedded in an elastic half space. *Proc. 13th Midwestern Mechanics Conf.* p. 333. University of Pittsburgh (1973).
11. B. Niumpradit and P. Karasudhi, Load transfer from an elastic pile to a saturated porous elastic soil. *Int. J. Numer. Anal. Methods Geomech.* **3**, 231 (1979).
12. V. Apirathvorakij and P. Karasudhi, Quasistatic bending of a cylindrical elastic bar partially embedded in a saturated elastic half space. *Int. J. Solids Structures* **16**, 625 (1980).
13. G. F. Fowler and G. B. Sinclair, The longitudinal harmonic excitation of a circular bar embedded in an elastic half space. *Int. J. Solids Structures* **14**, 999 (1978).
14. R. Parnes, Response of an elastically embedded rod subjected to periodically spaced longitudinal forces. *Int. J. Solids Structures* **17**, 891 (1981).
15. L. R. Herrmann, W. E. Mason and S. T. K. Chan, Response of reinforcing wires to compressive states of stress. *J. Compos. Mater.* **1**, 212 (1976).
16. A. P. S. Selvadurai, The flexure of an infinite strip of finite width embedded in an isotropic elastic medium of infinite extent. *Int. J. Numer. Anal. Methods Geomech.* **8**, 157 (1984).
17. M. C. Au and A. P. S. Selvadurai, On the flexure of an embedded structural element: A comparison of analytical and numerical estimates. *Proc. Southeastern Conf. Theor. Appl. Mech. XII* **1**, 143 (1984).
18. V. K. Luk and L. M. Keer, Stress analysis of a deep rigid axially loaded cylindrical anchor in an elastic medium. *Int. J. Numer. Anal. Methods Geomech.* **4**, 215 (1980).
19. A. P. S. Selvadurai, The load-deflection characteristics of a deep rigid anchor in an elastic medium. *Geotechnique* **26**, 603 (1976).

20. E. Sternberg, Load transfer and load diffusion in elastostatics. *Proc. 6th U.S. Nat. Cong. Appl. Mech.* p. 34, (1970).
21. G. M. L. Gladwell, *Contact Problems in the Classical Theory of Elasticity*. Sijthoff and Noordhoff, The Netherlands (1980).
22. R. Muki, Asymmetric problem of the theory of elasticity for a semi-infinite solid and a thick plate. *Progress in Solid Mechanics* (Edited by I. N. Sneddon and R. Hill) Vol. 1, p. 399. North Holland, Amsterdam; Interscience, New York (1960).
23. G. N. Watson, *A treatise on the theory of Bessel functions*. Cambridge University Press (1944).
24. G. Eason, B. Noble and I. N. Sneddon, On certain integrals of Lipschitz–Hankel type involving products of Bessel functions. *Philos. Trans. R. Soc. London, Ser. A* **247**, 529 (1955).
25. C. Heuman, Tables of complete elliptic integrals. *J. Math. Phys.* **20**, 127 (1941).
26. M. Abramowitz and I. A. Stegun, *Handbook of Mathematical Functions*. Dover, New York (1972).
27. P. Karasudhi, R. K. N. D. Rajapakse and B. Y. Hwang, Torsion of a long cylindrical elastic bar partially embedded in a layered elastic half space. *Int. J. Solids Structures* **20**, 1, (1984).
28. P. Karasudhi, R. K. N. D. Rajapakse and K. K. Liyanage, A reconsideration of load transfer problems involving a half space. *Trans. Can. Soc. Mech. Eng* (in press).
29. H. G. Poulos, Behaviour of laterally loaded piles; I—single piles. *J. Soil Mech. Found. ASCE* **97**, 711 (1971).

APPENDIX

The following are the expressions for displacements corresponding to concentrated ring forces shown in Fig. 3.

Concentrated vertical ring force [Fig. 3(a)]

$$w(r,z)=\frac{s}{8\mu(1-\nu)}\int_0^\infty\{[\lambda_1+\xi|z-z'|]e^{-\xi|z-z'|}+[\lambda_2+\lambda_1(z+z')\xi+2\xi^2zz']e^{-\xi(z+z')}\}J_0(\xi s)J_0(\xi r)d\xi$$

$$(0\le z,z'<\infty),\quad (A1)$$

$$u(r,z)=\frac{s}{8\mu(1-\nu)}\int_0^\infty\{\xi(z-z')e^{-\xi|z-z'|}+[-\lambda_3+\lambda_1(z-z')\xi+2\xi^2zz']e^{-\xi(z+z')}\}J_0(\xi s)J_1(\xi r)d\xi$$

$$(0\le z,z'<\infty).\quad (A2)$$

Concentrated radial ring force [Fig. 3(b)]

$$w(r,z)=\frac{s}{8\mu(1-\nu)}\int_0^\infty\{\xi(z'-z)e^{-\xi|z-z'|}+[-\lambda_3-\lambda_1(z-z')\xi+2\xi^2zz']e^{-\xi(z+z')}\}J_1(\xi s)J_0(\xi r)d\xi$$

$$(0\le z,z'<\infty),\quad (A3)$$

$$u(r,z)=\frac{s}{8\mu(1-\nu)}\int_0^\infty\{[\lambda_1-\xi|z-z'|]e^{-\xi|z-z'|}+[\lambda_2-\lambda_1(z+z')\xi+2\xi^2zz']e^{-\xi(z+z')}\}J_1(\xi s)J_1(\xi r)d\xi$$

$$(0\le z,z'<\infty).\quad (A4)$$

Concentrated ring force in x *direction* [Fig. 3(c)]

$$\frac{w(r,\theta,z)}{\cos\theta}=\frac{s}{8\mu(1-\nu)}\int_0^\infty\{\xi(z-z')\,e^{-\xi|z-z'|}+[\lambda_3+\lambda_1(z-z')\xi-2\xi^2zz']\,e^{-\xi(z+z')}\}J_0(\xi s)J_1(\xi r)\,d\xi$$

$$(0\le z,z'<\infty),\quad (A5)$$

$$\frac{u(r,\theta,z)}{\cos\theta}=\frac{s}{16\mu(1-\nu)}\int_0^\infty\{[\xi\,|\,z-z'\,|-\lambda_1]\,e^{-\xi|z-z'|}+[-\lambda_3+\lambda_1(z+z')\xi-2\xi^2zz']\,e^{-\xi(z+z')}\}$$
$$\times[J_2(\xi r)-J_0(\xi r)]J_0(\xi s)d\xi+\frac{s}{4\mu}\int_0^\infty[e^{-\xi|z-z'|}+e^{-\xi(z+z')}][J_2(\xi r)+J_0(\xi r)]J_0(\xi s)d\xi$$

$$(0\le z,z'<\infty),\quad (A6)$$

$$\frac{v(r,\theta,z)}{\sin\theta}=\frac{s}{16\mu(1-\nu)}\int_0^\infty\{[\xi\,|\,z-z'\,|-\lambda_1]\,e^{-\xi|z-z'|}+[-\lambda_3+\lambda_1(z+z')\xi-2\xi^2zz']\,e^{-\xi(z+z')}\}$$
$$\times[J_2(\xi r)+J_0(\xi r)]J_0(\xi s)d\xi+\frac{s}{4\mu}\int_0^\infty[e^{-\xi|z-z'|}+e^{-\xi(z+z')}][J_2(\xi r)-J_0(\xi r)]J_0(\xi s)d\xi$$

$$(0\le z,z'<\infty).\quad (A7)$$

Concentrated vertical ring force with azimuthal distribution [Fig. 3(d)]

$$\frac{w(r,\theta,z)}{\cos\theta}=\frac{s}{8\mu(1-\nu)}\int_0^\infty\{[\lambda_1+\xi\,|\,z-z'\,|]\,e^{-\xi|z-z'|}+[\lambda_3+\lambda_1(z+z')\xi$$
$$+2\xi^2zz']\,e^{-\xi(z+z')}\}J_1(\xi s)J_1(\xi r)\,d\xi\qquad(0\le z,z'<\infty),\quad (A8)$$

$$\frac{u(r,\theta,z)}{\cos\theta} = \frac{s}{16\mu(1-\nu)}\int_0^\infty \{\xi(z-z')\,e^{-\xi|z-z'|} + [-\lambda_3 + \lambda_1(z-z')\xi + 2\xi^2 zz']\,e^{-\xi(z+z')}\}[J_2(\xi r) - J_0(\xi r)]J_1(\xi s)\,d\xi \qquad (0 \le z, z' < \infty), \tag{A9}$$

$$\frac{v(r,\theta,z)}{\sin\theta} = \frac{s}{16\mu(1-\nu)}\int_0^\infty \{\xi(z-z')\,e^{-\xi|z-z'|} + [-\lambda_3 + \lambda_1(z-z')\xi + 2\xi^2 zz']\,e^{-\xi(z+z')}\}[J_2(\xi r) + J_0(\xi r)]J_0(\xi s)\,d\xi \qquad (0 \le z, z' < \infty), \tag{A10}$$

where

$$\lambda_1 = (3-4\nu); \qquad \lambda_2 = (8\nu^2 - 12\nu + 5); \qquad \lambda_3 = 4(1-\nu)(1-2\nu).$$

Influence functions for displacements due to distributed ring forces

The following influence functions for displacements are derived for the case of axial loading by integrating displacement expressions presented in eqns (A1)–(A4) across the thickness of a ring element.

If the jth element is a shaft element,

$$[f(r_i,z_i,s_j,z_j)]_v^{zs} = \frac{s_j}{8\mu(1-\nu)}\left[\int_{z'=z_j-\Delta t/2}^{z'=z_j+\Delta t/2}\{(\lambda+1)I_1(0,0;0) + (\lambda_2+\lambda_1)I_2(0,0;0)\}\,dz'\right] + \frac{s_j}{8\mu(1-\nu)}[(z_i-z')I_1(0,0;0) - \lambda_1(z_i+z')I_2(0,0;0) - 2z_iz'I_2(0,0;1) - 2z_iI_2(0,0;0)]_{z'=z_j-\Delta t/2}^{z'=z_j+\Delta t/2}, \tag{A11}$$

$$[f(r_i,z_i,s_j,z_j]_v^{rs} = \frac{s_j}{8\mu(1-\nu)}[\alpha(z_i-z')I_1(1,0;0) + I_1(1,0;-1) + (\lambda_3+\lambda_1)I_2(1,0;-1) - \lambda_1(z_i-z')I_2(0,0;0) - 2z_iz'I_2(1,0;1) - 2z_iI_2(1,0;0)]_{z'=z_j-\Delta t/2}^{z'=z_j+\Delta t/2}, \tag{A12}$$

$$[f(r_i,z_i,s_j,z_j]_r^{zs} = \frac{s_j}{8\mu(1-\nu)}[\alpha(z'-z_i)I_1(0,1;0) - I_1(0,1;-1) + (\lambda_3-\lambda_1)I_2(0,1;-1) + \lambda_1(z_i-z')I_2(0,1;0) - 2z_iz'I_2(0,1;1) - 2z_iI_2(0,1;0)]_{z'=z_j-\Delta t/2}^{z'=z_j+\Delta t/2}, \tag{A13}$$

$$[f(r_i,z_i,s_j,z_j]_r^{rs} = \frac{s_j}{8\mu(1-\nu)}[\alpha(\lambda_1-1)I_1(1,1;-1) - (z_i-z')I(1,1;0) - (\lambda_2-\lambda_1)I_2(1,1;-1) + \lambda_1(z_i+z')I_2(1,1;0) - 2z_iz'I(1,1;1) - 2z_iI(1,1;0)]_{z'=z_j-\Delta t/2}^{z'=z_j+\Delta t/2}. \tag{A14}$$

If the jth element is a base element,

$$[f(r_i,z_i,s_j,z_j)]_v^{zb} = \frac{1}{8\mu(1-\nu)}[s\{\lambda_1 I_1^*(0,1;-1) + (z_j-z_i)I_1^*(0,1;0) + \lambda_2 I_2^*(0,1;-1) + \lambda_1(z_i+z_j)I_2^*(0,1;0) + 2z_iz_jI_2^*(0,1;1)\}]_{s=s_j-\Delta b/2}^{s=s_j+\Delta b/2}, \tag{A15}$$

$$[f(r_i,z_i,s_j,z_j)]_v^{rb} = \frac{1}{8\mu(1-\nu)}[s\{(z_i-z_j)I_1^*(1,1;0) - \lambda_3 I_2^*(1,1;-1) + \lambda_1(z_i-z_j))I_2^*(1,1;0) + 2z_iz_jI_2^*(1,1;1)\}]_{s=s_j-\Delta b/2}^{s=s_j+\Delta b/2}, \tag{A16}$$

$$[f(r_i,z_i,s_j,z_j)]_r^{zb} = \frac{1}{8\mu(1-\nu)}[s^2\{(z_j-z_i)I_1^*(0,2;0) - \lambda_3 I_2^*(0,2;-1) - \lambda_1(z_i-z_j)I_2^*(0,2;0) + 2z_iz_jI_2^*(0,2;1)\}]_{s=s_j-\Delta b/2}^{s=s_j+\Delta b/2}, \tag{A17}$$

$$[f(r_i,z_i,s_j,z_j)]_r^{rb} = \frac{1}{8\mu(1-\nu)}[s^2\{\lambda_1 I_1^*(1,2;-1) - (z_j-z_i)I_1^*(1,2;0) + \lambda_2 I_2^*(1,2;-1) - \lambda_1(z_i+z_j)I_2^*(1,2;0) + 2z_iz_jI_2^*(1,2;1)\}]_{s=s_j-\Delta b/2}^{s=s_j+\Delta b/2}. \tag{A18}$$

In eqns (A11)–(A14),

$$\alpha = \begin{cases} -1 & \text{if } z_i < z_j - \Delta t/2, \\ 1 & \text{if } z_i > z_j + \Delta t/2. \end{cases} \tag{A19}$$

If $z_j - \Delta t/2 < z_i < z_j + \Delta t/2$, then the influence functions given in eqns (A11)–(A14) should be computed by considering the integration over the interval $[z_j - \Delta t/2,\ z_j + \Delta t/2]$ as summation of integration over the intervals $[z_j - \Delta t/2,\ z_i]$ and $[z_i,\ z_j + \Delta t/2]$ with appropriate value of α given by eqn (A19).

In eqns (A11)–(A18)

$$I_1(m,n;p) = \int_0^\infty J_m(\xi r_i)J_n(\xi s_j)\xi^p\,e^{-\xi|z_i-z'|}\,d\xi, \tag{A20}$$

$$I_2(m, n;p) = \int_0^\infty J_m(\xi r_i)J_n(\xi s_j)\xi^p \, e^{-\xi(z_i+z')} \, d\xi, \tag{A21}$$

$$I_1^*(m, n;p) = \int_0^\infty J_m(\xi r_i)J_n(\xi s)\xi^p \, e^{-\xi(z_j-z_i)} \, d\xi; \tag{A22}$$

$$I_2^*(m, n;p) = \int_0^\infty J_m(\xi r_i)J_n(\xi s)\xi^p \, e^{-\xi(z_j+z_i)} \, d\xi. \tag{A23}$$

The following influence for displacements are derived for the case of lateral and moment loading by integrating the displacement expressions presented in eqns (A5)–(A10), across the thickness of a ring element.

If the jth element is a shaft element,

$$[f(r_i, z_i, s_j, z_j)]_v^{zs} = \frac{s_j}{8\mu(1-\nu)}[\alpha(\lambda_1+1)I_1(1,1;-1) + (z_i - z')I_1(1,1;0) - (\lambda_1+\lambda_2)I_2(1,1;-1) - \lambda_1(z_i+z')I_2(1,1;0) - 2z_iz'I_2(1,1;1) - 2z_iI_2(1,1;0)]_{z'=z_j-\Delta t/2}^{z'=z_j+\Delta t/2}, \tag{A24}$$

$$[f(r_i, z_i, s_j, z_j)]_v^{rs} = \frac{s_j}{16\mu(1-\nu)}[\alpha(z_i - z')\{I_1(2,1;0) - I_1(0,1;0)\} + I_1(2,1;-1) - I_1(0,1;-1) + (\lambda_1+\lambda_3)\{I_2(2,1;-1) - I_2(0,1;-1)\} - \lambda_1(z_i - z')\{I_2(2,1;0) - I_2(0,1;0)\} - 2z_iz'\{I_2(2,1;1) - I_2(0,1;1)\} - 2z_i\{I_2(2,1;0) - I_2(0,1;0)\}]_{z'=z_j-\Delta t/2}^{z'=z_j+\Delta t/2}, \tag{A25}$$

$$[f(r_i, z_i, s_j, z_j)]_x^{zs} = \frac{s_j}{8\mu(1-\nu)}[-(z_i - z')I_1(1,0;0) + I_1(1,0;-1) - (\lambda_3-\lambda_1)I_2(1,0;-1) + \lambda_1(z' - z_i)I_2(1,0;0) + 2z_iz'I_2(1,0;1) + 2z_iI_2(1,0;0)]_{z'=z_j-\Delta t/2}^{z'=z_j+\Delta t/2}, \tag{A26}$$

$$[f(r_i, z_i, s_j, z_j)]_x^{rs} = \frac{s_j}{16\mu(1-\nu)}\left[\int_{z_j-\Delta t/2}^{z_j+\Delta t/2}\{(\lambda_1-1)I_1(0,0;0) + (\lambda_2-\lambda_1)I_2(0,0;0) + 4(1-\nu)I_1(0,0;0) + 4(1-\nu)I_2(0,0;0)\}\,dz'\right] + \frac{s_j}{16\mu(1-\nu)}[-\alpha_1(\lambda_1-1)I_1(2,0;-1) + (z_i - z')\{I_1(2,0;0) - I_1(0,0;0)\} + (\lambda_2-\lambda_1)I_2(2,0;-1) - \lambda_1(z_i+z')\{I_2(2,0;0) - I_2(0,0;0)\} + 2z_iz'\{I_2(2,0;1) - I_2(0,0;1)\} + 2z_i\{I_2(2,0;0) - I_2(0,0;0)\} + 4(1-\nu)\{-\alpha_1I_1(2,0;-1) - I_2(2,0;-1)\}]_{z'=z_j-\Delta t/2}^{z'=z_j+\Delta t/2}. \tag{A27}$$

If the jth element is a base element,

$$[f(r_i, z_i, s_j, z_j)]_v^{zb} = \frac{1}{8\mu(1-\nu)}[s^2\{\lambda_1I_1^*(1,2;-1) + (z_j - z_i)I_1^*(1,2;0) + \lambda_2I_2^*(1,2;-1) + \lambda_1(z_i+z_j)I_2^*(1,2;0) + 2z_iz_jI_2^*(1,2;1)\}]_{s=s_j-\Delta b/2}^{s=s_j+\Delta b/2}, \tag{A28}$$

$$[f(r_i, z_i, s_j, z_j)]_v^{rb} = \frac{1}{16\mu(1-\nu)}[s^2\{(z_i - z_j)[I_1^*(2,2;0) - I_1^*(0,2;0)] - \lambda_3[I_2^*(2,2;-1) - I_2^*(0,2;-1)] + \lambda_1(z_i - z_j)[I_2^*(2,2;0) - I_2^*(0,2;0)] + 2z_iz_j[I_2^*(2,2;1) - I_2^*(0,2;1)]\}]_{s=s_j-\Delta b/2}^{s=s_j+\Delta b/2}, \tag{A29}$$

$$[f(r_i, z_i, s_j, z_j)]_x^{zb} = \frac{1}{8\mu(1-\nu)}[-(z_j - z_i)I_1^*(1,1;0) + \lambda_3I_2^*(1,1;-1) + \lambda_1(z_i - z_j)I_2^*(1,1;0) - 2z_iz_jI_2^*(1,1;1)]_{s=s_j-\Delta b/2}^{s=s_j+\Delta b/2}, \tag{A30}$$

$$[f(r_i, z_i, s_j, z_j)]_x^{rb} = \frac{1}{16\mu(1-\nu)}[-\lambda_1\{I_1^*(2,1;-1) - I_1^*(0,1;-1)\} + (z_j - z_i)\{I_1^*(2,1;0) - I_1^*(0,1;0)\} - \lambda_2\{I_2^*(2,1;-1) - I_2^*(0,1;-1)\} - 2z_iz_j\{I_2^*(2,1;1) - I_2^*(0,1;1)\} + \lambda_1(z_i+z_j)\{I_2^*(2,1;0) - I_2^*(0,1;0) + 4(1-\nu)\{I_2^*(2,1;-1) + I_2^*(0,1;-1) + I_1^*(2,1;-1) + I_1^*(0,1;-1)\}]_{s=s_j-\Delta b/2}^{s=s_j+\Delta b/2}. \tag{A31}$$